Zuerst erschienen in: International Journal of Pressure Vessels and Piping 82 (2005), Seite 217–225
http://dx.doi.org/10.1016/j.ijpvp.2004.07.022

Local and global collapse pressure of longitudinally flawed pipes and cylindrical vessels

M. Staat*

Aachen University of Applied Sciences, Div. Jülich, Ginsterweg 1, 52428 Jülich, Germany

Abstract

Limit loads can be calculated with the finite element method (FEM) for any component, defect geometry, and loading. FEM suggests that published long crack limit formulae for axial defects under-estimate the burst pressure for internal surface defects in thick pipes while limit loads are not conservative for deep cracks and for pressure loaded crack-faces. Very deep cracks have a residual strength, which is modelled by a global collapse load. These observations are combined to derive new analytical local and global collapse loads. The global collapse loads are close to FEM limit analyses for all crack dimensions.

Keywords: Limit analysis; Global and local collapse; Axially cracked pipe; Pressure loaded crack-face

1. Introduction

Many burst tests with flawed pipes and vessels indicate that the burst pressure could be predicted by plastic limit analysis [1–3]. Limit load formulae are needed for defect assessment by the two criteria methods [4–8] or the engineering treatment method [9]. In the reference stress approach, they can be used to estimate nonlinear fracture mechanics parameters such as crack tip opening displacement (CTOD), J and C^* integrals [7,10].

Plastic limit loads for axial defects in pipes have been collected in Refs. [11,12]. A new type of local and global collapse loads has been derived in Ref. [13] combining the solutions for long defects and for slits. However, the formulae in Refs. [4,12,13] are not correct. Burst tests could be explained by limit analysis for a wide range of materials and of the dimensions of pipes and defects in Ref. [2]. However, Ref. [2] also showed that existing global collapse loads need to be further improved and proposed some ad hoc improvements. In Ref. [14], new global formulae have been obtained by approximation to incremental finite element limit analyses for thin pipes.

In this contribution, corrections of the thick pipe limit loads in Ref. [12] are made. They are then used to derive improved global and local collapse loads for thick pipes in the sense of Refs. [4,5,13]. The global collapse loads are compared to lower bound finite element limit loads with and without pressure loading on internal cracks. The results are used to suggest also new local collapse loads. In Ref. [3], the new global collapse loads are compared to 278 burst tests with thick and thin-walled pipes.

Reliable limit loads are important, because over-estimating burst pressure is clearly non-conservative. However, under-estimating limit loads could also be non-conservative, because it leads to under-predicting CTOD and crack opening area and consequently also to under-predicting leak rates.

1.1. Limit analysis

Stresses $\boldsymbol{\sigma}$ are admissible in a perfectly plastic material model, if they satisfy the Tresca or the von Mises yield condition $F(\boldsymbol{\sigma}) \leq \sigma_y$. With equality $F(\boldsymbol{\sigma}) = \sigma_y$ in one point, the elastic limit (0.2% strain limit) $\sigma_y = R_{p0.2}$ is assumed and yielding can begin there. In the context of the two-surface theory of plasticity, the yield surface $F_Y(\boldsymbol{\sigma}) \leq \sigma_y = R_{p0.2}$ can harden kinematically within a bounding surface $F_U(\boldsymbol{\sigma}) \leq \sigma_u$

* Tel.: +49 2461 99 3209; fax: +49 2461 99 3199.
E-mail address: m.staat@fh-aachen.de.

Nomenclature

a	crack length
c	crack depth
D	constraint factor
E	Young's modulus
eps	relative prognosis error
F_Y, F_U	yield function, bounding function
f	function
M_{FL}	Folias factor
M_1, M_2	Folias factor for internal and external defect
$\boldsymbol{n}$	exterior unit normal
P	reference pressure
$\bar{p}_0$, p_0	burst pressure without defect old, new
p_{exp}, $p_{formula}$	experimental, predicted burst pressure
$\bar{p}_{global}$, p_{global}	global collapse pressure old, new
$\bar{p}_{local}$, p_{local}	local collapse pressure old, new
$\bar{p}_L$, p_L	collapse pressure of defect pipe old, new
R_1^*, R_1	distinction of crack-face loading old, new
r_1, r_2	interior and exterior radius, respectively
$R_{p0.2}$	0.2% proof stress
R_m	ultimate stress
t	wall thickness
γ	limit load factor
Ω	body
$\partial\Omega_\sigma$	traction boundary
$\boldsymbol{\sigma}$	stress tensor
σ_y	yield stress
σ_u	ultimate stress
σ_F	flow stress

with some ultimate stress σ_u. In the simplest theory, the bounding surface is assumed as fixed in size, form, and location in stress space. Usually the same function is used for both surfaces, i.e. $F(\boldsymbol{\sigma}) = F_Y(\boldsymbol{\sigma}) = F_U(\boldsymbol{\sigma})$.

The structure Ω is loaded monotonically by the surface traction p on the traction boundary $\partial\Omega_\sigma$. For simplicity of the presentation, the body forces are neglected. The tractions are proportional to the internal pressure p. Starting from some reference pressure P, one may ask for the load factor $\gamma > 1$ by which P can be increased up to the collapse pressure $p_L = \gamma P$. The limit load p_L of a bounded kinematic hardening material can be computed exactly by the maximum problem, [15],

$$\begin{aligned} &\text{maximize } \gamma, \quad \text{such that} \quad F(\boldsymbol{\sigma}) \le \sigma_u \text{ in } \Omega, \\ &-\operatorname{div}\boldsymbol{\sigma} = \mathbf{0} \text{ in } \Omega, \quad \boldsymbol{\sigma n} = \gamma P \mathbf{n} \text{ on } \partial\Omega_\sigma. \end{aligned} \tag{1}$$

The finite element discretisation of this optimization problem has been implemented in the finite element method (FEM) software PERMAS [16] and solved by a basis reduction technique. The numerical method of the limit analysis is presented in detail in Ref. [15]. The linear matching method has been developed from the elastic compensation method as an alternative for FEM limit analysis [17]. Compared to the basis reduction method, the elastic compensation method is more easily programmed but it seems to have some difficulties to converge [18].

The maximum problem (1) shows that the burst pressure p_L is homogeneous of first order in σ_u. Therefore, one may write in non-dimensional similarity variables

$$\frac{p_L}{\sigma_u} = Df(a/t, a/c, t/r_1, r_2/r_1, \ldots). \tag{2}$$

Here, the crack size is characterised by crack depth a and crack length 2c as shown in Fig. 1. The pipe geometry is characterised by r_1, r_2 and t which are internal and external radius and wall thickness. The constraint factor D distinguishes the yield condition

$$D = \begin{cases} 1 & \text{for Tresca,} \\ \dfrac{2}{\sqrt{3}} & \text{for von Mises} \end{cases} \tag{3}$$

for problems of pressurised pipes without defects.

Often the limit load analysis is only understood in a perfectly plastic context with $\sigma_u = \sigma_y = R_{p0.2}$ and the fictitious failure load is called the limit load. Eq. (1) shows that the yield stress has no influence for kinematic

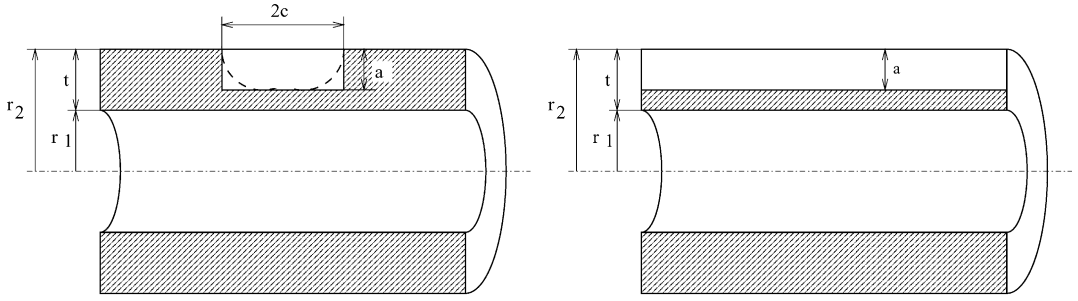

(a) Axial, external surface defect. (b) Long axial external defect in a pipe.

Fig. 1. External semi-elliptical surface defect and infinitely long defect in a pipe.

hardening material and that the actual load at failure is the ultimate load calculated with some σ_u. In the two criteria methods, only partial use is made of hardening by setting σ_u equal to the flow stress σ_F,

$$\sigma_u = \sigma_F = \frac{R_{p0.2} + R_m}{2}. \tag{4}$$

In 300 burst tests with pipes with axial defects, this was a best choice [3]. Limit analysis predicts only global collapse load. The local collapse load is sometimes related with ligament (or net-section) collapse. As the ligament thickness tends to zero with $a \to t$, the local collapse load tends to zero. However, the pipe may still carry the limit load, i.e. the global collapse load.

2. The extreme cases

2.1. Thick pipe without defect

The burst pressure p_0 of the thick-walled pipe without defects is

$$\frac{p_0}{\sigma_u} = D \ln\frac{r_2}{r_1} = D \ln\left(1 + \frac{t}{r_1}\right)$$
$$= D\left[\frac{t}{r_1} - \frac{1}{2}\left(\frac{t}{r_1}\right)^2 + \frac{1}{3}\left(\frac{t}{r_1}\right)^3 - \cdots\right], \tag{5}$$

which must be assumed asymptotically by realistic limit load solutions for the cracked pipe. Therefore, the constraint factor D is introduced in all equations below, although it is originally omitted in most of the equations that have been cited from different references. The series expansion (5) converges for $t/r_1 \le 1$. The solution for the Tresca yield function applies independently of the conditions at the pipe end. The solution for the hypothesis after von Mises does not apply to the open pipe with free ends.

The approximation

$$\frac{\bar{p}_0}{\sigma_u} = D\frac{t}{r_1} \tag{6}$$

for thin pipes over-estimates the load-carrying capacity of thick pipes, as the series expansion (5) shows. For $\nu = 0.3$, the assumption of small deformations applies and therefore Eq. (5) remains valid with the Tresca hypothesis up to $r_2/r_1 = 5.43$ for closed ends [19]. The limits in which the relation is valid with the von Mises hypothesis are discussed in Ref. [19]. In the following, a closed pipe is assumed.

2.2. Pipes with penetrating axial cracks

For the collapse load of wall penetrating longitudinal cracks, semi-empirical formulae were set-up, which are often called Battelle formula or slit curve in the literature. According to Refs. [1,20], the burst pressure of the penetrating axial crack can be written in the form

$$\frac{\bar{p}_L}{\sigma_u} = D\frac{t}{r_1 M_{FL}}. \tag{7}$$

A simple relation for the Folias factor M_{FL} is

$$M_{FL} = \sqrt{1 + 1.61\frac{c^2}{r_1 t}}. \tag{8}$$

For $c \to 0$, $M_{FL} \to 1$. The burst pressure must then become the load (5) for the uncracked pipe. Therefore, it is suggested to generalise the Battelle formula (7) by

$$\frac{p_L}{\sigma_u} = \frac{D}{M_{FL}} \ln\frac{r_2}{r_1} \tag{9}$$

for thick pipes. This modification is supported by the FEM limit analyses for penetrating defects (i.e. $a/t = 1$, most obviously for $a/c > 0.4$).

2.3. Long axial cracks in pipes

A lower bound for the limit load of a thick pipe with a long defect is obtained, if the pipe is divided into two coaxial pipes Pipe 1 carries the defect (slit pipe) and is stress free. Pipe 2 is a pipe thinned by a and is at yield in all of its points.

By this consideration, the collapse load

$$\lim_{c\to\infty}\frac{\bar{p}_L}{\sigma_u} = D\left[\left(\frac{r_1}{R_1^*}\right)\ln\left(\frac{r_2}{r_1 + a}\right)\right] \tag{10}$$

with

$$R_1^* = \begin{cases} r_1 & \text{pressure} - \text{excluding crack faces,} \\ r_1 + a & \text{pressure} - \text{including crack faces} \end{cases} \tag{11}$$

was presented for the internal crack with $R_1^* = r_1$ in Ref. [12]. That is a lower bound solution with a piecewise continuous effective stress field such that $F(\sigma(r)) = \sigma_u$ for $r_1 + a < r < r_2$. This incorrectly assumes that the internal pressure acts on a cylinder of radius $r_1 + a$. By correcting $r_1 + a$ to the internal pipe radius r_1

$$\lim_{c\to\infty}\frac{p_L}{\sigma_u} = D\left[\left(\frac{r_1}{R_1}\right)\left(\frac{r_1 + a}{r_1}\right)\ln\left(\frac{r_2}{r_1 + a}\right)\right] \tag{12}$$

equilibrium is achieved at least for the hoop stress. It is less conservative to replace R_1^* with R_1,

$$R_1 = \begin{cases} r_1 & \text{pressure} - \text{excluding crack faces,} \\ r_1 + \dfrac{a}{2} & \text{pressure} - \text{including crack faces.} \end{cases} \tag{13}$$

The limit load for the external defect

$$\lim_{c\to\infty}\frac{p_L}{\sigma_u} = D \ln\left(\frac{r_2 - a}{r_1}\right) \tag{14}$$

is correct in Ref. [12].

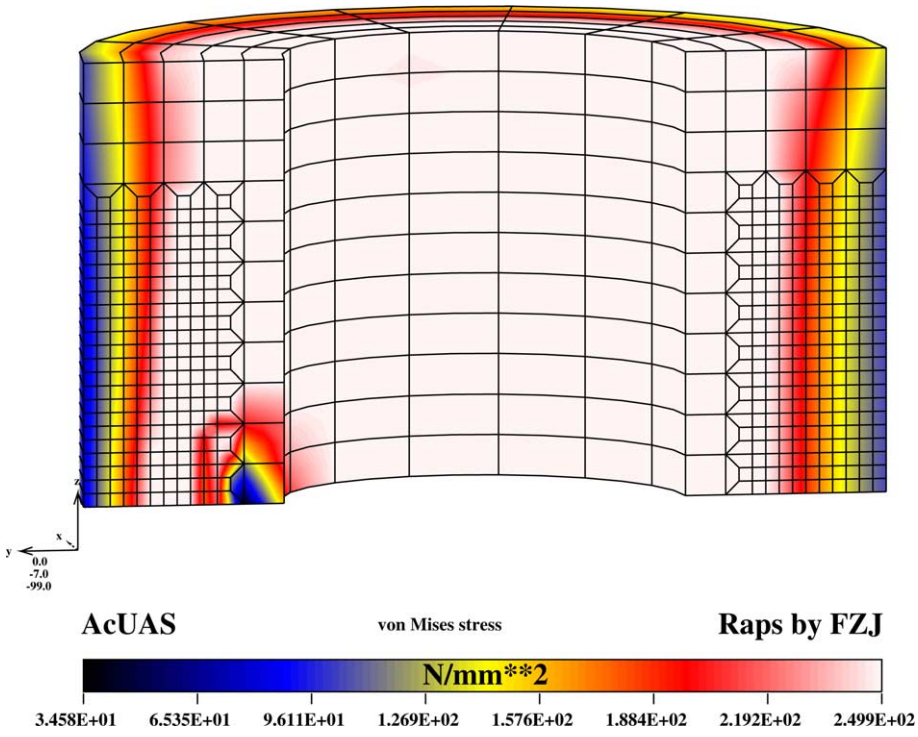

Fig. 2. FEM mesh and von Mises stress for internal defect in a thick pipe ($r_2/r_1=2$) with $\sigma_y=\sigma_u=250$ N mm^{-2}. The defect causes unloading behind the crack front.

3. Global collapse of pipes containing axial surface defects

3.1. Global collapse of pipes containing internal defects

A lower bound of the global limit load dependent on the defect position is obtained, by dividing the pipe into two coaxial pipes, which together are in static equilibrium with the internal pressure [12]. Pipe 1 contains the surface crack as a penetrating defect. Pipe 2 is intact with a collapse load after Eq. (5). In this way, the collapse load for the thick pipe with an internal axial surface crack has been obtained in Refs. [12,13]

$$\frac{\bar{p}_{global}}{\sigma_u} = D\left[\frac{a}{r_1 M_1} + \left(\frac{r_1}{R_1^*}\right)\ln\left(\frac{r_2}{r_1 + a}\right)\right] \tag{15}$$

with the Folias factor M_1

$$M_1 = \sqrt{1 + 1.61\frac{c^2}{r_1 a}} \tag{16}$$

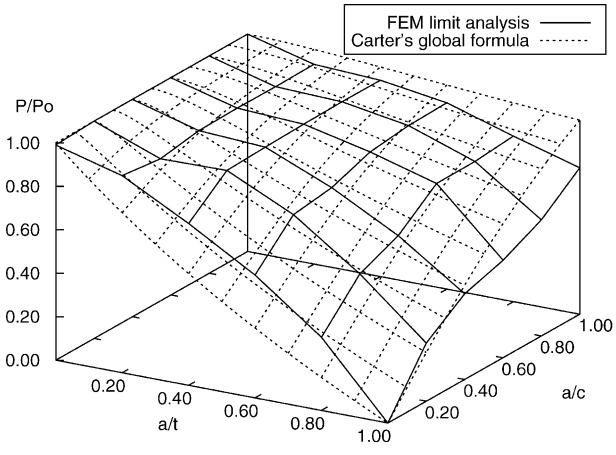

(a) Sealed crack faces, $R_1^* = r_1$.

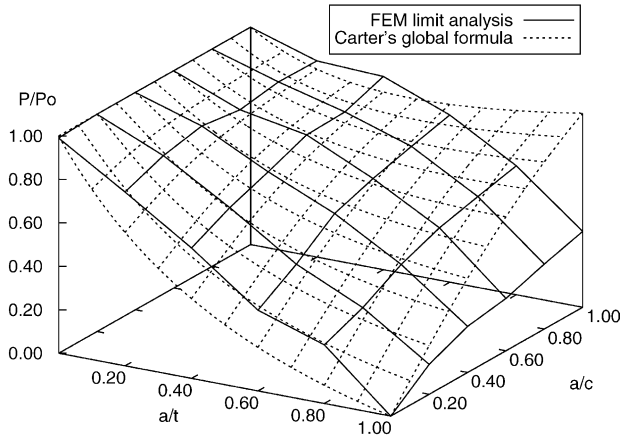

(b) Pressure on crack faces, $R_1^* = r_1 + a$.

Fig. 3. Carter's global collapse pressure ($\bar{p}_{global}$, Eq. (15)) compared with FEM limit analyses for internal defects in a thick pipe with $r_2/r_1=2$. FEM —, formula ⋯. The pressures are normalised by p_0.

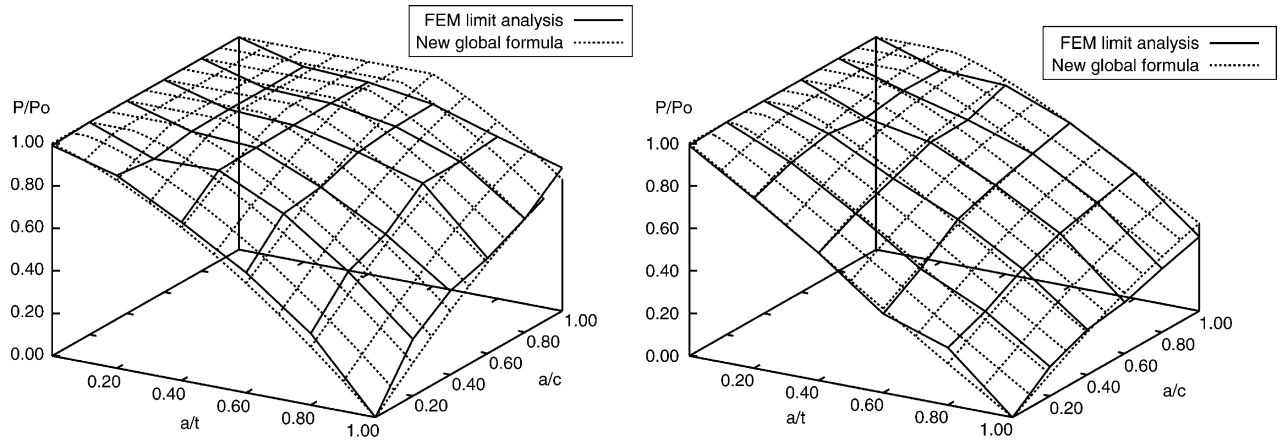

(a) Sealed crack faces, $R_1 = r_1$. (b) Pressure on crack faces, $R_1 = r_1 + a/2$.

Fig. 4. New global collapse pressure (p_{global}, Eq. (17)) compared with FEM limit analyses for internal defects in a thick pipe with $r_2/r_1 = 2$. FEM —, formula ···. The pressures are normalised by p_0.

using Eqs. (7) and (10). R_1^* makes the distinction of cases of crack-face loading of Eq. (11) for the long defect part of the solution only.

The global collapse pressure is extensively checked against lower bound FEM limit analyses with rectangular and semi-elliptical defects. A typical FEM net of an internal defect in a thick-walled pipe with $r_2/r_1 = 2$ is shown in Fig. 2. Only one quarter of the pipe has been modelled, because of the symmetry of the problem. The rectangular defect causes unloading behind the crack front. There is no need for special crack tip elements or for mesh refinement, because of plastic collapse is not controlled by the crack tip. All analyses have been repeated with thin-walled pipes ($r_2/r_1 = 1.1$) with both types of crack shape, rectangular and semi-elliptical. These show similar trends but the differences between FEM limit analysis, old and new collapse formulae are less pronounced for thin pipes. The formulae have been derived for rectangular defects. Therefore, they are compared with FEM solutions for this crack shape.

The global collapse pressure (15), normalised with the burst pressure $p_0 = \sigma_u D \ln(r_2/r_1)$ of the pipe without a defect, is compared with FEM limit analyses in Fig. 3 for a thick-walled pipe with $r_2/r_1 = 2$. The long crack limit (10), i.e. $c \to \infty$ or $a/c \to 0$, under-estimates the burst pressure. But the deep crack solution ($a/t > 0.8$) is not conservative for shorter defects with $a/c > 0.4$. Moreover, the pressure on the crack-faces is not considered for deep cracks such that the solution greatly over-estimates the burst pressure for all defect shapes a/c as is obvious from Fig. 3(b).

By use of the corrected Eqs. (9) and (12) an improved global collapse load is found

$$\frac{p_{global}}{\sigma_u} = D \min\left\{ \ln\left(\frac{r_2}{r_1}\right); \left(\frac{r_1}{R_1}\right)\left[\frac{1}{M_1}\ln\left(\frac{r_1 + a}{r_1}\right) + \left(\frac{r_1 + a}{r_1}\right)\ln\left(\frac{r_2}{r_1 + a}\right)\right]\right\}. \tag{17}$$

Here, the effect of pressure on the crack-faces is also correctly considered on the slit part of the solution. As limit value for $c \to \infty$ one obtains the new lower bound (12) for the local collapse because $M_1 \to \infty$.

Fig. 4 shows that Eq. (17) greatly improves the global collapse load for all limiting cases, for deep or long internal defects. The new long crack limit (12) is a close lower bound. For sealed crack-faces in Fig. 4(a), the solution

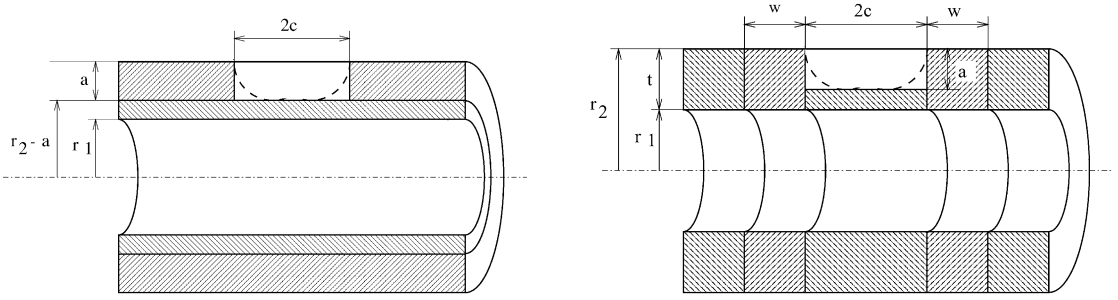

(a) Partition for global collapse. (b) Partition for local collapse.

Fig. 5. Sections of different continuous stress fields at plastic collapse of an external axial surface crack in a pipe.

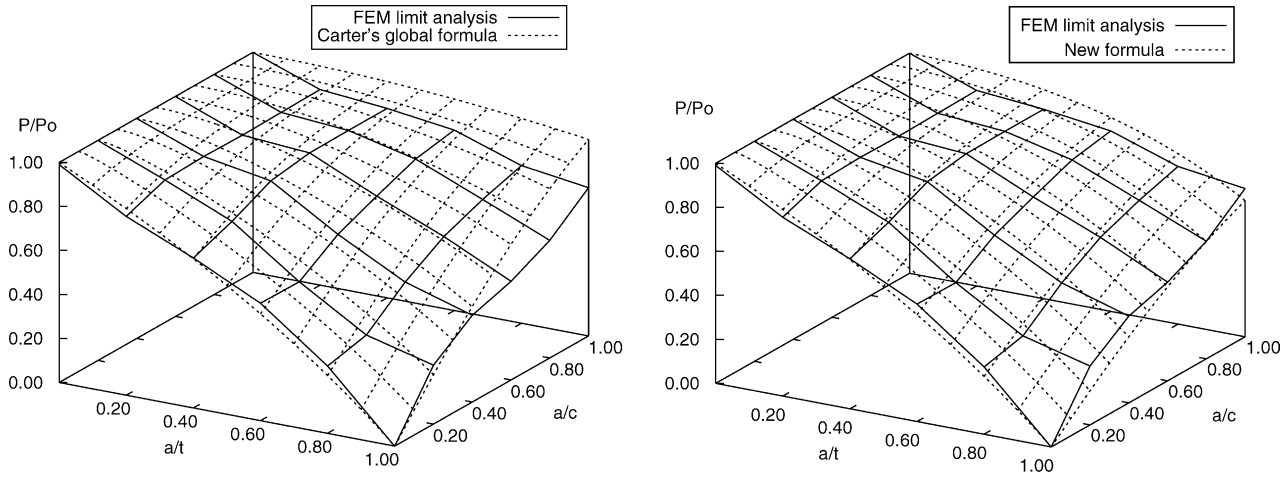

(a) Carter's global formula $\bar{p}_{global}$ (18). (b) New global formula p_{global} (20).

Fig. 6. Global collapse pressure formulae compared with FEM analyses for external defects in a thick pipe with $r_2/r_1 = 2$. FEM —, formula ···. The pressures are normalised by p_0.

needs to be bounded by $p_0 = \sigma_u D \ln(r_2/r_1)$ for small defects. Fig. 4(b) shows that the new solution (17) is accurate for pressurised crack-faces for all parameters and that the limit p_0 hardly becomes active.

3.2. Global collapse of pipes containing external defects

In Refs. [4,13], the partition into sections as shown in Fig. 5(a) leads to a piecewise continuous stress field which has been used to derive global collapse loads for the thick pipe with an axial surface crack at the external wall

$$\frac{\bar{p}_{global}}{\sigma_u} = D\left[\frac{a}{(r_2 - a)M_2} + \ln\left(\frac{r_2 - a}{r_1}\right)\right] \tag{18}$$

with the Folias factor M_2

$$M_2 = \sqrt{1 + 1.61\frac{c^2}{(r_2 - a)a}}. \tag{19}$$

This can be improved if Eq. (7) is replaced by Eq. (9) such that

$$\frac{p_{global}}{\sigma_u} = D\left[\frac{1}{M_2}\ln\left(\frac{r_2}{r_2 - a}\right) + \ln\left(\frac{r_2 - a}{r_1}\right)\right]. \tag{20}$$

With finite c Eqs. (15) and (20) approach the solution (9) of the penetrating defect for $a \to t$. As limit value for $c \to \infty$, one obtains the lower bound of Eq. (12) for local collapse because $M_2 \to \infty$.

The modification of Eq. (18) in Eq. (20) concerns only the thick wall correction of the slit solution. The difference can be observed for the wall penetrating defect ($a/t = 1$) in Fig. 6.

The new global formula (20) has been compared to 278 burst tests with external or penetrating defects in Ref. [3]. Fig. 7 shows that the relative prognosis error eps,

$$\text{eps} = \frac{p_{exp} - p_{formula}}{p_{formula}} \tag{21}$$

increases by its definition for long, deep defects due to uncertainties of geometric and material data ($\text{eps} \to \infty$ for $p_{formula} \to 0$ and $0 < p_{formula} < p_{exp}$; $\text{eps} \to -1$ for $p_{formula} \to 0$ and $p_{formula} > p_{exp} > 0$). Therefore, conservative data have to be used in defect assessment. Probabilistic fracture mechanics is a modern alternative [21].

All FEM limit analyses have been checked with internal and external semi-elliptical defects. Fig. 8 for external defects shows that the FEM limit analyses with rectangular defects are slightly conservative with respect to semi-elliptical defect shapes. The differences are smaller for thin pipes.

4. Local collapse of pipes containing axial surface defects

4.1. Local collapse of pipes containing internal defects

For the thick pipe with an internal semi-elliptical surface crack in the longitudinal direction local collapse loads are given[1] in Refs. [4,13]

$$\frac{\bar{p}_{local}}{\sigma_u} = \frac{D}{s_1 + c}\left[s_1 \ln\left(\frac{r_2}{r_1}\right) + c\left(\frac{r_1}{R_1^*}\right)\ln\left(\frac{r_2}{r_1 + a}\right)\right] \tag{22}$$

along with

$$s_1 = \frac{ca\left(1 - \frac{a}{t}\right)}{M_1 r_1\left[\ln\left(\frac{r_2}{r_1}\right) - \left(\frac{r_1}{R_1^*}\right)\ln\left(\frac{r_2}{r_1 + a}\right)\right] - a} \tag{23}$$

and the distinction of cases of crack-face loading (11).

[1] A misprint in Ref. [4], p. AII.36, has been corrected in Eq. (22).